

Parametric downconversion and optical quantum gates: two's company, four's a crowd

M. Barbieri^{a,*†}, T.J. Weinhold^{a,b}, B.P. Lanyon^a, A. Gilchrist^{a,c}, K.J. Resch^{a,d}, M.P. Almeida^a and A.G. White^a

^aCentre for Quantum Computer Technology, Department of Physics, University of Queensland, QLD, Brisbane, Australia;

^bCentre for Quantum Dynamics, Griffith University, Brisbane, QLD, Australia; ^cDepartment of Physics, Macquarie University, Sydney Australia; ^dInstitute for Quantum Computing, University of Waterloo, Canada

(Received 26 February 2008; final version received 30 June 2008)

We show that the primary cause of errors in a broad class of optical quantum-logic gates are due to the higher-order photon terms in parametric downconversion sources. A model describing real-life imperfections in these entangling gates is presented and tested in an experiment where we entangle dependent photons from the same downconversion source using a controlled- z gate, and measure the state tomographically. We find good agreement between the modelled and measured results. Our investigations demonstrate that, although small, these noise terms are amplified by the intrinsic non-determinism of the gates. It is worth considering alternative schemes based on weak nonlinearities to see if they are more resilient to this degradation.

Keywords: entanglement generation; linear optical computing; parametric downconversion

1. Introduction

Quantum computing promises computational power beyond that possible with the current paradigm based on classical information theory. Driven by this, many different physical systems have been explored experimentally, including atoms [1], ions [2,3], superconducting circuits [4], and photons [5]. All of them satisfy some necessary requirements for being a scalable architecture [6], but still several technical problems have to be efficiently solved. Photons are particularly attractive, since they are robust against decoherence, and can be easily initialised in high-purity states. The main limitation comes from their exceedingly small intrinsic interaction strength. In fact, the entangling gates necessary for quantum computing require strong coupling between qubits. A solution has been found in the combination of linear-optical elements, measurement, and feedforward: by a measurement-induced nonlinearity it is possible to achieve deterministic entangling gates [7]. There are known paths to a scalable architecture, both in the conventional circuit model [5,7], and measurement-based computation using cluster states [8–10]. Linear optical entangling gates have been shown to be highly

performing [11], accurately characterised [12] and fast with respect to the qubit decoherence time [13].

The above optical quantum computing schemes assume the availability of Fock states, that is, single photons in a well-defined spatio-temporal mode. Such sources are not yet available experimentally and state-of-the-art practice is to use pairs of photons generated in spontaneous parametric downconversion (SPDC), where measurement of a photon in one mode flags the presence of a single photon in the correlated mode [14]. Although a good approximation, this does not provide a true single-photon source, since the pairs of photons are generated spontaneously and there is a finite probability of two or more pairs being produced. This probability scales with the source brightness, which due to better coupling efficiency and new nonlinear materials has increased six orders of magnitude since the first demonstration of SPDC [15]. Consequently, the deviation from the single-photon approximation can be quite significant.

Here we investigate the effect of using SPDC photons in linear optical entangling gates. To date such gates have been used for entangled *state* generation, for instance in cluster synthesis, and in the circuit model, where the quality of the entangling *process* is

*Corresponding author. Email: marco.barbieri.qo@gmail.com

† Present address: Laboratoire C. Fabry, Institute d'Optique, 91127 Palaiseau, France

paramount. We focus on the generation of entangled states; we quantify the outputs by using tomography [16], and compare them to our model which accounts for higher-order photon terms, circuit imperfections, and photon loss. Different from previous studies [17], our model is not limited to obtaining a prediction of the non-classical interference visibility, but provides an expression for state tomography outcomes. We show that in current experiments noise due to higher-order photons terms quickly becomes the dominant error as source brightness is increased, overwhelming the errors expected due to mode mismatch.

2. Experiment

We implement an entangling gate, the controlled- z gate (cz), which ideally consists of a non-classical interferometer where one polarisation component of each photon can interfere, and the orthogonal components

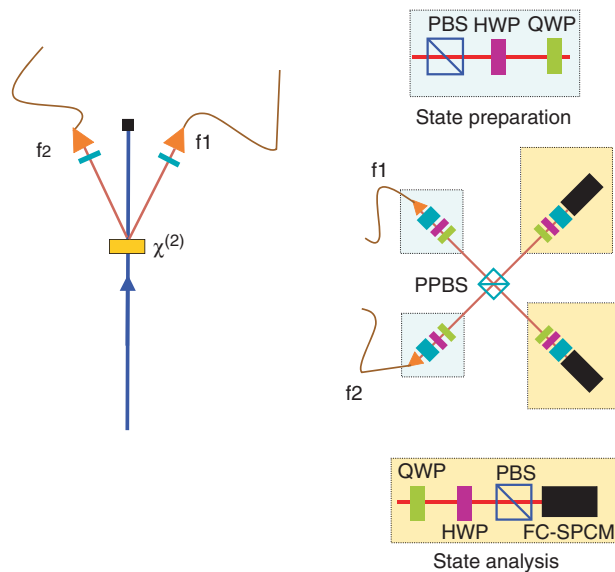


Figure 1. Schematic of the two-photon down conversion source and of the optical entangling gate. A frequency doubled laser beam ($\lambda_p = 410$ nm, duration 100 fs, repetition rate 80 MHz) excites downconversion in a $\chi^{(2)}$ crystal. Photons are generated on modes $f1$ and $f2$. The light is frequency filtered ($\Delta\lambda = 3$ nm), and coupled to single-mode fibers. In the experiment we used a 2 mm BiB_3O_6 (BiBO) crystal. The qubits are encoded in photon polarisation, states are prepared and analysed using a combination of a polariser (PBS), a quarter-wave plate (QWP), and a half-wave plate (HWP) [16]. The entangling gate is based on a single partially polarising beam splitter (PPBS), selective interference leads to a controlled sign shift (details in the text) [22–24]. Photons are detected by fibre-coupled counting modules (FC-SPCM, model Perkin-Elmer AQR-14 FC), connected to a twofold coincidence circuit. (The colour version of this figure is included in the online version of the journal.)

do not interact. Such gates have been realised with Jamin–Lebedev interferometers [12,18–21], with partial-polarising beam splitters [11,22–26], and with integrated optics [27]. Figure 1 shows a schematic of the realisation we use here: single photons meet at the surface of a partially polarising beam splitter (PPBS), whose reflectivities for the horizontal, H , and vertical, V , polarisations are ideally $\eta_H = 1/3$ and $\eta_V = 1$. If both photons are vertically polarised no interference occurs; if both are horizontally polarised non-classical interference occurs resulting in a π -phase shift. The input states are pre-biased to compensate for the intrinsic polarisation-dependent loss, i.e. single photons polarised in each output as $|\bar{D}\rangle = (\sqrt{3}|H\rangle + |V\rangle)/2$ will ideally give the maximally entangled output state $|\Phi^+\rangle = (|HA\rangle - |VD\rangle)/\sqrt{2}$, where D and A represent diagonal and anti-diagonal polarisation.

Tomographic measurements of the states are obtained by a series of projective polarisation measurements [28]. The high twofold count rate allows us to adopt an overcomplete set of measurements, $\{p, q\}$, where $p, q \in \{H, V, D, A, R, L\}$, and R and L are the right- and left-circular polarisations. The overcomplete set is desirable as it is more accurate and more resilient to noise [29]. As it has been seen in previous experiments, we found that the states were not perfect, although close to the ideal. To understand why this is the case, we model three key components: the source, the optical circuit, and photon losses.

3. Model

3.1. Source

Parametric downconversion is one of the most widely used technologies for producing single photons and photon pairs. Although the modes from downconversion are well defined in terms of frequency, polarisation, and spatial and temporal extent, they suffer a range of undesired features: there is a wide frequency bandwidth making coupling to atomic or ionic transitions difficult; the efficiency of downconversion is low, of the order of 10^{-2} , which limits timing control, and since it is a spontaneous process there is no control of photon number¹. For a given polarisation and spatiotemporal mode, the downconversion output can be expressed as a power series,

$$|\psi\rangle_{SPDC} = \left(A_f a_{f1}^\dagger a_{f2}^\dagger + \frac{A_f^2}{2} (a_{f1}^\dagger)^2 (a_{f2}^\dagger)^2 + \dots \right) |0\rangle|0\rangle, \quad (1)$$

where $a_{f1}^\dagger, a_{f2}^\dagger$ are creation operators of the two downconversion modes, and A_f^n is the probability amplitude of producing n pairs of photons; the probability, $|A_f|^2$,

is linearly proportional to the pump intensity [30]. Here we truncate the expansion to neglect terms higher than two pairs due to their small effect.

3.2. Optical circuit

The components in the optical circuit are engineered with a range of precisions: the polarising beam splitters are Glan–Taylor, with extinction ratios of 10^{-5} ; the half- and quarter-waveplates induce relative phase shifts which are correct to within $\pm 2^\circ$; the partial-polarising beam splitter has measured reflectivities of $\eta_H=0.35$, instead of $1/3$ and $\eta_V=0.99$, instead of 1 . The Glan–Taylor beam splitter introduces negligible error compared to the other components. Errors introduced by waveplates can be compensated either in the experiment by additional waveplate elements, or in the analysis by numerical rotation of the states – we do the latter here. The errors introduced by the PPBS cannot be corrected so we model its effect by using the following mode transformations, $\mathbf{U}_{\text{gate}}^\dagger$:

$$\begin{aligned} \bar{a}_{1,x}^\dagger &= \sqrt{1-\eta_x} a_{1,x}^\dagger + i\sqrt{\eta_x} a_{2,x}^\dagger, \\ \bar{a}_{2,x}^\dagger &= \sqrt{1-\eta_x} a_{2,x}^\dagger + i\sqrt{\eta_x} a_{1,x}^\dagger, \end{aligned} \quad (2)$$

where a_1^\dagger, a_2^\dagger are the input modes, $\bar{a}_1^\dagger, \bar{a}_2^\dagger$ the output modes, and the index $x=H,V$ identifies the polarisation. In the alternative Jamin–Lebedev architecture the reflectivities can be tuned with far greater precision [18], but this is less appealing in the long term as it is more difficult to implement in micro-optical devices. Better precision PPBS could be obtained by use of more expensive bulk-optics, or by moving to well-engineered micro-optics [27].

3.3. Photon loss

Photons can be lost due to inefficiencies in fibre coupling, both before and after the PPBS, reflections and absorption in the optical components ($\lesssim 0.5\%$ per component), reflection and absorption in the frequency filters ($\sim 50\%$ per filter over the whole bandwidth), and limited efficiency in the photon counters (at 820 nm we lose $\sim 40\%$). Due to the linearity of our circuit, we can model the combined effect of the losses by assuming lossless components and introducing a beam splitter in front of the detectors, where its transmittivity is the probability for a photon to survive in that mode. We assume that the transmittivity is the same for both polarisations.

We are only considering cases with at least one photon in each output mode – in the absence of higher-

order terms we could disregard loss as it would only reduce the number of events. However, as we shall see, the combination of loss and multi-pair emissions affects the signal-to-noise ratio in a more complex fashion. Experimentally, losses in the mode $j=\{f1,f2\}$ can be estimated from the coincidence to singles ratio. The photon loss probability is given by

$$k_j = 1 - \frac{C_{j,l} - A_{j,l}}{S_l - B_l}, \quad (3)$$

where the coincidence count rate between modes j, l , $C_{j,l}$ is corrected for accidental counts, $A_{j,l}$, and the singles count rate in mode l , S_l , is corrected for background counts, B_l ; all parameters are measured directly. Our gates operate in a high loss regime. In our experiment, $k_{f1}=0.929$, $k_{f2}=0.946$: here we do not correct for accidentals or background since they are negligible. The effect of the losses is modelled by a polarisation-insensitive beam splitter with transmittivity $\sqrt{k_j}$ on each mode; the corresponding transform $\mathbf{U}_{\text{loss}}^\dagger$ affects the input mode as

$$a_j^\dagger \rightarrow \sqrt{k_j} a_j^\dagger + i\sqrt{1-k_j} a_{j,\text{loss}}^\dagger. \quad (4)$$

For the gate input, we need to consider two different loss modes for each polarisation; therefore, we have four loss modes.

3.4. The full model

We propagate the input state through the PPBS, $\mathbf{U}_{\text{gate}}^\dagger$, and losses, $\mathbf{U}_{\text{loss}}^\dagger$ (where the loss beam splitters introduce an extra mode for each polarisation of each output), obtaining the output state,

$$|\psi\rangle_{\text{out}} = \mathbf{U}_{\text{loss}}^\dagger \mathbf{U}_{\text{gate}}^\dagger (|\psi\rangle_{SPDC} |0\rangle_{\text{loss}}^{\otimes 4}), \quad (5)$$

where $|0\rangle_{\text{loss}}^{\otimes 4}$ represents the loss modes for the orthogonal polarisations of each spatial mode. At the gate input, the state preparation is set so that both spatial modes are \bar{D} -polarised. We compute the coincidence probability for polarisation analysers set to $\{p,q\}$ in the two output arms, which simulates the outcome of a tomographic measurement. Since the detectors cannot discriminate between single- and multi-photon events, we consider all terms containing at least one photon in both detection modes, and add the respective probabilities. We do not have to add the amplitudes, as these terms are in principle distinguishable and hence do not interfere. As described above, our model of the source only considers up to four-photon terms, so the following detection events will lead to a coincidence in our model: the desired signal $\langle 1|_p \langle 1|_q$, and the noise terms $\langle 1|_p \langle 2|_q$, $\langle 2|_p \langle 1|_q$, $\langle 2|_p \langle 2|_q$, $\langle 1|_p \langle 3|_q$, and $\langle 3|_p \langle 1|_q$. Note

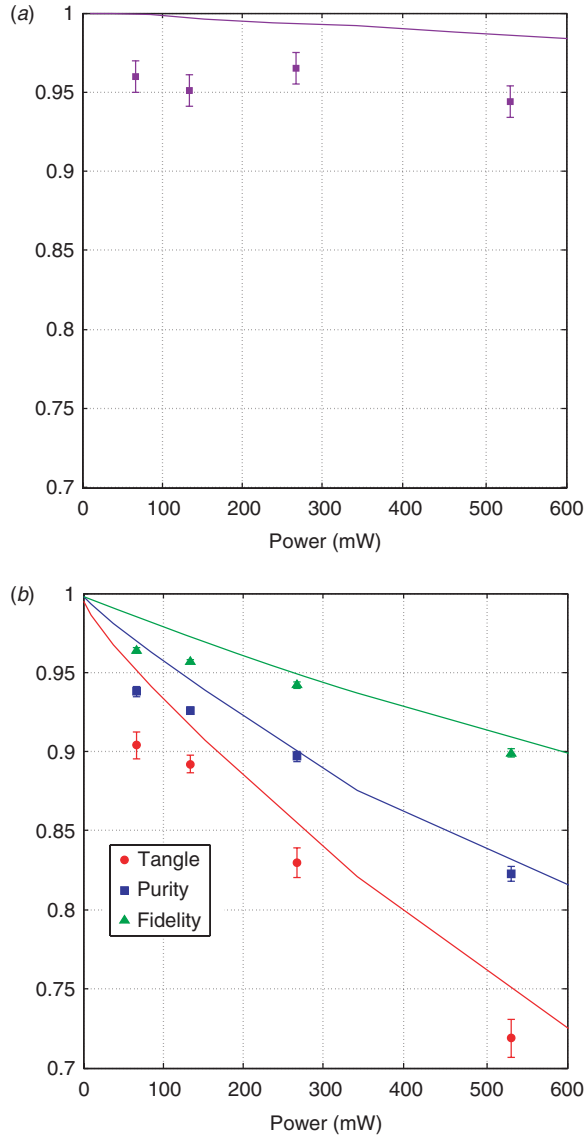


Figure 2. (a) Relative visibility of non-classical interference versus downconversion pump power, $\mathcal{V}_{\text{rel}} = \mathcal{V}_{\text{meas}}/\mathcal{V}_{\text{ideal}}$, where $\mathcal{V}_{\text{meas}}$ and $\mathcal{V}_{\text{ideal}}$ are the measured and ideal visibilities, respectively. The solid line is predicted by our model based on dependent photons, incorporating higher-order terms and loss. The errors in the measured visibilities are obtained from a Gaussian fit. (b) The fidelity, purity, and tangle [16,28] of the output state of the gate versus pump power for the input beams polarised as $\hat{D} = (\sqrt{3}H + V)/2$. Solid lines are the predictions of the model, errors in the measured data are obtained from a Monte Carlo simulation [12,28]. The non-unity values at zero power are due to the measured PPBS reflectivities of $\eta_H = 0.35$, $\eta_V = 0.99$. Count rates were ranging from 2 kHz at high power to 150 Hz at the lowest power, measured after the gate. (The colour version of this figure is included in the online version of the journal.)

that the tomographic procedure assumes that the coincidence signal is purely due to the $\langle 1|_p \langle 1|_q$ term, which is why the higher-order terms show as noise in this reduced Hilbert space.

4. Analysis

Linear optical quantum gates work due to non-classical interference. A standard gauge of gate performance is to compare the visibility of the measured non-classical interference to the expected value, $\mathcal{V}_{\text{rel}} = \mathcal{V}_{\text{meas}}/\mathcal{V}_{\text{ideal}}$. Here, the expected value, $\mathcal{V}_{\text{ideal}}$, is calculated using the measured beam splitter reflectivity $\eta_H = 0.35$, and by analyzing only the H components. The visibility is degraded by photon distinguishability: here we explicitly account for the degradation due to higher-order photon terms, but do not account for distinguishability due to mode mismatch, be it spatial, temporal, or frequency. Figure 2(a) plots the relative visibility versus power for the dependent photon case; the solid line is the prediction from our model and the data points are measured at four different powers. The model predicts a small decrease in visibility with increasing power; the measured data are offset by an approximately constant amount, which we attribute to mode mismatch. Both the predicted and measured changes in visibility due to the increasing power are of the order of a few percent. Note that in our model there is only interference between the two photons in the $|1\rangle_{1,H}|1\rangle_{2,H}$ term or the four photons in the $|2\rangle_{1,H}|2\rangle_{2,H}$ term [31,32] – if there were no losses, the latter term could be ruled out by photon-number resolving detection and there would be no decrease in visibility with power. At all powers, the dominant source of noise is mode mismatch, it being only at high powers that the noise due to higher-order terms begins to play a significant role. A reasonable – but it turns out incorrect – expectation would be that quantum logic gates, whose operation intrinsically relies on non-classical interference, would likewise be affected.

In the dependent case we are interested in the quality of the state produced by the gate, e.g. for cluster state production. Entangled state quality can be measured in several ways: the fidelity of the reconstructed state ρ with the ideal $F = \langle \Phi^+ | \rho | \Phi^+ \rangle$; the degree of purity of the state; and the degree of entanglement, as measured by the tangle [16,28]. The model's predictions for these parameters are shown by the solid lines in Figure 2(b). It is striking how severely the quality of the state is affected by the higher-order photon terms. This behavior is qualitatively different to the non-classical visibility, since here the dominant source of noise is due to the higher-order terms. This is due to the non-deterministic nature of the entangling gate. Consider inputting the term $|1\rangle_{1,H}|1\rangle_{2,V}$. Even with no subsequent losses to the gate, the photons may not make it to the detectors due to the intrinsic failure probability of the gate – in such a case, a coincidence will not be registered. However, now consider the higher-order term, $|2\rangle_{1,H}|2\rangle_{2,V}$ – the

intrinsic loss of the gate can populate the output modes to produce, e.g. $|1\rangle_{1,H}|1\rangle_{2,H}$, which produces a coincidence, albeit an erroneous one in quantum-logic terms. Thus, non-deterministic quantum-logic gates are much more susceptible to higher-order photon terms than non-classical visibility. Clearly, the data follow the trend predicted by the model. At low powers there is an offset, which is expected since as the power goes to zero we expect our measures to trend to the values solely due to mode-mismatch. We have also observed that in more complicated circuits with lower success probability the effect of higher-order terms becomes even more deleterious [11], again as expected.

Scalable optical quantum computing requires both independent photons and arbitrary input states – neither condition is met in the previous model and experiment. Independent photon sources can be obtained by triggered downconversion [33]; the entangling-gates process can be quantified by quantum process tomography. Such an experiment has been reported in [26]; here the model has been applied to obtain an error budget per gate in linear optical architecture, and relate it to the threshold for fault tolerance. As before, the model considers the effect of higher-order terms, circuit imbalances, and loss: the fidelity between the model and measured matrices is very high, $F_p = 0.967 \pm 0.015$. Poor gate performance is primarily due to higher-order photon terms, and we attribute the difference of 3.2% to mode mismatch. It has been noted that if this were the only source of error, then the gate would be in a fault-tolerant regime [26]. With multiplexing and photon-number-resolving detection it is predicted that the higher-order terms could be reduced by several orders of magnitude [33]. There is a residual 2.8% drop in gate performance due to incorrect beam splitter reflectivity: this can be reduced by at least an order of magnitude with better fixed-reflectivity optics or tunable optics, as mentioned above.

In conclusion, we have shown that the primary cause of error in an entire class of optical entangling gate experiments [11,12,18–27] is higher-order photon terms. This is at first a surprising result given how small these terms are in practice; however, we have shown that their effects are greatly magnified by the non-deterministic function of linear optical entangling gates. These can be limited by reducing the brightness of the downconversion source; nevertheless, this solution would amplify other sources of noise, such as mechanical stability of the setup and long-term power fluctuations. This can also affect the quality of the state and process reconstruction due to lower counts. A previous theoretical analysis of alternative linear-optical schemes [34–36] found broadly similar

results, noting that gates with higher symmetry suffered less, even if they had lower success probability [17]. Our results highlight once more the critical importance of developing better single-photon sources and photon-number-resolving detectors for linear-optical schemes. We suggest that alternative schemes for optical quantum computing, such as measurement-amplified nonlinearities [37] or Zeno gates [38], may suffer less from amplification of the higher-order terms since they are intrinsically near-deterministic; the former scheme also enjoys the advantage that the photonic qubits can, in principle, be fully distinguishable. It remains to be seen to what extent these alternative architectures relax the constraints on single-photon sources. In the Zeno schemes, for example, losses degrade the performance of the gate itself [39], unlike in the linear-optical schemes.

Acknowledgements

This work was supported by the Australian Research Council Discovery and Federation Fellow programs, the DEST Endeavour Europe program, and an IARPA-funded US Army Research Office Contract.

Note

1. Paraphrasing Winston Churchill: parametric downconversion is the worse possible technology for a single photon source, with the exception of all the others.

References

- [1] Mandel, O.; Greiner, M.; Wildera, A.; Rom, T.; Hänsch, T.H.; Bloch, I. *Nature*. **2003**, *425*, 937–940.
- [2] Schmidt-Kaler, F.; Häffner, H.; Riebe, M.; Gulde, S.; Lancaster, G.P.T.; Deuschle, T.; Becher, C.; Roos, C.F.; Eschner, J.; Blatt, R. *Nature*. **2003**, *422*, 408–411.
- [3] Leibfried, D.; DeMarco, B.; Meyer, V.; Lucas, D.; Barrett, M.; Britton, J.; Itano, W.M.; Jelenković, B.; Langer, C.; Rosenband, T.; Wineland, D.J. *Nature*. **2003**, *422*, 412–415.
- [4] Plantenberg, H.J.; de Groot, P.C.; Harmans, C.J.P.M.; Mooij, J.E. *Nature*. **2007**, *447*, 836–839.
- [5] Kok, P.; Munro, W.J.; Nemoto, K.; Ralph, T.C.; Dowling, J.P.; Milburn, G.J. *Rev. Mod. Phys.* **2007**, *79*, 135–174.
- [6] Di Vincenzo, D.P. *Science*. **1995**, *270*, 255–261.
- [7] Knill, E.; Laflamme, R.; Milburn, G.J. *Nature*. **2001**, *409*, 46–52.
- [8] Raussendorf, R.; Briegel, H.J. *Phys. Rev. Lett.* **2001**, *86*, 5188–5191.
- [9] Nielsen, M.A. *Phys. Rev. Lett.* **2004**, *93*, 040503-1–4.
- [10] Walther, P.; Resch, K.J.; Rudolph, T.; Schenck, E.; Weinfurter, H.; Vedral, V.; Aspelmeyer, M.; Zeilinger, A. *Nature*. **2005**, *434*, 169–176.

- [11] Lanyon, B.P.; Barbieri, M.; Almeida, M.P.; Jennewein, T.; Ralph, T.C.; Resch, K.J.; Pryde, G.J.; O'Brien, J.L.; Gilchrist, A.; White, A.G. 2008, arXiv:0804.0272.
- [12] O'Brien, J.L.; Pryde, G.J.; Gilchrist, A.; James, D.F.V.; Langford, N.K.; Ralph, T.C.; White, A.G. *Phys. Rev. Lett.* **2004**, *93*, 080502-1-4.
- [13] Prevedel, R.; Walther, P.; Tiefenbacher, F.; Böhil, P.; Kaltenbaek, R.; Jennewein, T.; Zeilinger, A. *Nature* **2007**, *445*, 65-69.
- [14] Burnham, D.C.; Weinberg, D.L. *Phys. Rev. Lett.* **1970**, *25*, 84-87.
- [15] Fedrizzi, A.; Herbst, T.; Poppe, A.; Jennewein, T.; Zeilinger, A. *Optics Express* **2007**, *15*, 15377-15386.
- [16] James, D.F.V.; Kwiat, P.G.; Munro, W.J.; White, A.G. *Phys. Rev. A* **2001**, *64*, 052312-1-15.
- [17] Gilchrist, A.; Munro, W.J.; White, A.G. *Phys. Rev. A* **2003**, *67*, 040304(R)-1-4.
- [18] O'Brien, J.L.; Pryde, G.J.; White, A.G.; Ralph, T.C.; Branning, D. *Nature* **2003**, *426*, 264-267.
- [19] Pryde, G.J.; O'Brien, J.L.; White, A.G.; Bartlett, S.D.; Ralph, T.C. *Phys. Rev. Lett.* **2004**, *92*, 190402-1-4.
- [20] Pryde, G.J.; O'Brien, J.L.; White, A.G.; Ralph, T.C.; Wiseman, H.M. *Phys. Rev. Lett.* **2005**, *94*, 220405-1-4.
- [21] Pryde, G.J.; O'Brien, J.L.; White, A.G.; Bartlett, S.D. *Phys. Rev. Lett.* **2005**, *94*, 220406-1-4.
- [22] Langford, N.K.; Weinhold, T.J.; Prevedel, R.; Resch, K.J.; Gilchrist, A.; O'Brien, J.L.; Pryde, G.J.; White, A.G. *Phys. Rev. Lett.* **2005**, *95*, 210504-1-4.
- [23] Kiesel, N.; Schmid, C.; Weber, U.; Ursin, R.; Weinfurter, H. *Phys. Rev. Lett.* **2005**, *95*, 210505-1-4.
- [24] Okamoto, R.; Hofmann, H.F.; Takeuchi, S.; Sasaki, K. *Phys. Rev. Lett.* **2005**, *95*, 210506-1-4.
- [25] Lanyon, B.P.; Weinhold, T.J.; Langford, N.K.; Barbieri, M.; James, D.F.V.; Gilchrist, A.; White, A.G. *Phys. Rev. Lett.* **2007**, *99*, 250505-1-4.
- [26] Weinhold, T.J.; Gilchrist, A.; Resch, K.J.; Doherty, A.C.; O'Brien, J.L.; Pryde, G.J.; White, A.G. *Understanding photonic quantum-logic gates and the road to fault tolerance*. 2008, arXiv:0808.0794.
- [27] Politi, A.; Cryan, M.J.; Rarity, J.G.; Yu, S.; O'Brien, J.L. *Science* **2008**, *320*, 646-649.
- [28] White, A.G.; Gilchrist, A.; Pryde, G.J.; O'Brien, J.L.; Bremner, M.J.; Langford, N.K. *J. Opt. Soc. Am. B* **2007**, *24*, 172-183.
- [29] Langford, N.K. Ph.D. Thesis, University of Queensland. 2007.
- [30] Yariv, A. *Quantum Electronics* 3rd ed.; John Wiley & Sons: New York, 1989.
- [31] Sanaka, K.; Resch, K.J.; Zeilinger, A. *Phys. Rev. Lett.* **2006**, *96*, 083601-1-4.
- [32] Resch, K.J.; O'Brien, J.L.; Weinhold, T.J.; Sanaka, K.; Lanyon, B.P.; Langford, N.K.; White, A.G. *Phys. Rev. Lett.* **2007**, *98*, 203602-1-4.
- [33] Migdall, A.L.; Branning, D.; Castelletto, S. *Phys. Rev. A* **2002**, *66*, 053805-1-4.
- [34] Ralph, T.C.; White, A.G.; Munro, W.J.; Milburn, G.J. *Phys. Rev. A* **2001**, *65*, 012314-1-6.

- [35] Knill, E. *Phys. Rev. A* **2002**, *66*, 052306-1-5.
- [36] Pittman, T.B.; Jacobs, B.C.; Franson, J.D. *Phys. Rev. Lett.* **2002**, *88*, 257902-1-4.
- [37] Nemoto, K.; Munro, W.J. *Phys. Rev. Lett.* **2004**, *93*, 250502-1-4.
- [38] Franson, J.D.; Jacobs, B.C.; Pittman, T.B. *Phys. Rev. A* **2004**, *70*, 062302-1-13.
- [39] Myers, C.R.; Gilchrist, A. *Phys. Rev. A* **2007**, *75*, 052339-1-5.

Appendix 1

We sketch how to obtain the emission probability from coincidence measurements. This is evaluated by a comparison of the number of coincidences in a given polarisation, with one PPBS input arm blocked and with both arms unblocked. When injecting the state $|\Psi_{SPDC}\rangle$, with both photons polarised along the H direction, the coincidence counts can be written as

$$C_{11} \propto A_f^2 M_{11} + A_f^4 M_{22}, \quad (6)$$

where M_{11} and M_{22} are the probabilities of obtaining a coincidence count when injecting a single pair or a double pair, respectively. M_{11} has a simple expression

$$M_{11} = \langle 1|_H \langle 1|_H \rho_{\text{out}} |1\rangle_H |1\rangle_H, \quad (7)$$

where ρ_{out} is the state after partial trace on the loss modes

$$\rho_{\text{out}} = \text{Tr}_{\text{loss}} |\psi_1\rangle \langle \psi_1|, \quad (8)$$

with

$$|\psi_1\rangle = U_{\text{loss}}^\dagger U_{\text{gate}}^\dagger (a_{f_1}^\dagger a_{f_2}^\dagger) |0\rangle |0\rangle. \quad (9)$$

The expression for M_{22} is more complicated, due to the fact that detectors cannot distinguish single-photon events and two-photon events; this can be evaluated numerically once the measured values for the reflectivities η_H and η_V and the losses k_{f_1} and k_{f_2} are included. When one input arm is blocked, only higher-order photons can give a coincidence count C_{20} , so we can write

$$C_{20} \propto A_f^4 M_{20}, \quad (10)$$

where M_{20} is now evaluated starting from the input state $(a_{f_1}^\dagger)^2 |0\rangle |0\rangle$, and carrying out the same numerical evaluation as for M_{22} . Notice that we are implicitly assuming that the losses are the same in both arms. We can assume this, introducing only a small error as the measured values k_{f_1} and k_{f_2} confirm. The ratio of Equations (6) and (10) allows us to estimate the amplitude A_f . In our experiment, we found: $A_f=0.051$ for 65 mW; $A_f=0.073$ for 130 mW; $A_f=0.103$ for 260 mW; and $A_f=0.147$ for 530 mW. In these regimes, the expected higher-order term contributions are 0.25%, 0.48%, 1.05%, and 2.06%, respectively.